

THE EFFECT OF SEABED PROPERTIES ON THE RECEIVE BEAM PATTERN OF A HYDROPHONE LOCATED ON THE SEAFLOOR

Miles J.G. Parsons and Alec J. Duncan

Centre for Marine Science and Technology, Curtin University, GPO Box U1987, Perth, WA 6845, Australia

Multi-path interference is often considered when modelling propagation of underwater sounds from source to receiver. When close to, or on the seabed, a hydrophone receives the direct and bottom reflected signals at nearly identical times. The resulting interference leads to an effective receive beam pattern that depends not only on source and receiver position and water depth, but also on the seabed characteristics, which affect the phase and magnitude of the reflection coefficient. Numerical acoustic propagation models account for this phenomenon automatically, however; it is important that it be taken into account when received signals are used to carry out simple calculations of source levels of nearby sources based on spherical spreading. Australian waters lie above seabeds of greatly differing acoustic properties. Compressional and shear sound speeds and absorption properties for four bottom types (basalt, calcarenite, sand and silt) were used to model the effective receive beam pattern of a hydrophone located on the seafloor. Modelling was carried out for all four seabeds as well as a seabed comprising differing thicknesses of sand over a calcarenite half space. The effects of the resulting receive beam pattern on estimations of source levels and locations are discussed.

INTRODUCTION

Underwater noise levels have increased significantly over the last few decades and the implications for marine fauna are far reaching [1-3]. Measurement and modelling of ambient noise and the source levels of biological and anthropogenic sounds are now conducted on a regular basis to evaluate impacts of sound on behaviour and hearing of animals, monitor movements of vocalising species and observe any reactions to environmental influences such as temperature and salinity [4-7].

The propagation of underwater sound is complex and dependent on numerous variables, such as source and receiver position, water depth, temperature and salinity profiles, multi-path interference and seabed acoustic properties [8].

For ease of long-term recording, and to reduce flow noise, hydrophones are often positioned on, or near, the seabed [9]. However, the combination of direct, reflected and head waves (waves that travel through the seabed and re-radiate into the water column) affect the receive beam pattern of the hydrophone. It is therefore not possible to assume that, in this position, a hydrophone is omni-directional and it is necessary to model the receive beam pattern to accurately understand the recorded sound pressure levels. Numerical acoustic propagation models automatically incorporate this effect, so it is of little consequence in situations where the positions of the source and receiver are known, information about the acoustic properties of the seabed is available, and it is practical to numerically calculate the transmission loss between source and receiver [10]. However, in bioacoustic experiments it is often the case that the source position, and particularly its height above the seabed, is unknown, and the seabed properties are only known approximately [11]. It is therefore important that this phenomenon be understood so that appropriate bounds can be put on source levels estimated from these experiments.

There has been little work done to estimate the effects of differing seabeds on the effective receive beam pattern of a hydrophone in close-proximity to the seafloor. The aim of this study was therefore to model the likely vertical plane receive pattern of a hydrophone on four typical seabeds found in waters around Australia. The impacts these receive patterns would have on estimates of range and source level were also investigated

METHODS

If the incident sound is a plane wave of amplitude p_0 , then it is straightforward to show that the received pressure at a hydrophone a height h above the seabed is given by:

$$p = p_0(1 + \Re(\Theta)\exp(2ikh \sin \Theta)) \quad (1)$$

where $\Re(\Theta)$ is the complex plane-wave pressure reflection coefficient, k is the acoustic wavenumber, and Θ is the grazing angle (the angle between the wave vector and the plane of the seabed). (A time dependence of $\exp(-i\omega t)$ has been assumed.)

A number of computer programs exist that are capable of calculating the pressure reflection coefficient of a seabed consisting of an arbitrary number of fluid and elastic layers, so this leads to a simple method of calculating an equivalent vertical plane beam pattern, which is given by:

$$b(\Theta) = \frac{p}{p_0} = 1 + \Re(\Theta)\exp(2ikh \sin \Theta) \quad (2)$$

In the limiting case of a hydrophone much closer to the seabed than the acoustic wavelength, $kh \ll 1$ and

$$b(\Theta) \approx 1 + \Re(\Theta) \quad (3)$$

The results of plane wave reflection coefficient and phase for

each seabed presented in this paper were calculated using the plane wave reflection coefficient calculation program BOUNCE [12] via the AcTUP user interface [13].

Brekovskikh and Lysanov [14] deal in detail with seabed reflections of sound from point sources and show that in many practical cases the plane wave assumption is invalid as it ignores important transmission paths, particularly the head or lateral wave that enters the seabed at some distance from the receiver and propagates along the interface while re-radiating into the water column, and the Scholte wave, which is a low-speed wave that propagates along the interface between a fluid and an elastic medium. To account for these effects a numerical modelling approach was used to calculate the beam pattern as a function of both grazing angle and slant range for a hydrophone positioned 1 cm above the seabed. This was done by using the fast-field program, SCOOTER [12] to calculate the transmission losses between a source on the seabed and a grid of receiver locations spanning the desired horizontal ranges and grazing angles. This is a very efficient calculation and the principle of acoustic reciprocity ensures that transmission losses calculated in this way are the same as those between a grid of sources and a single receiver on the seabed [15]. Sea surface reflections were reduced to negligible levels by making the water depth 1000m. Once the transmission loss grid was calculated it was converted to an equivalent beam pattern by expressing each value as a pressure ratio and multiplying by

the corresponding slant range between the source and receiver. Finally, these values were binned onto a uniform grazing angle.

A limitation of this method is that SCOOTER uses an exponential approximation to the Hankel function that is invalid at horizontal separations between the source and receiver that are less than a wavelength. This placed an upper limit on the maximum grazing angle at which beam pattern values for a given range could be calculated. Another assumption is that the direct, reflected and head waves all arrive within a time difference much less than the source signal duration, so that that the signals travelling via these different paths overlap.

Results obtained using SCOOTER were verified for both fluid and elastic half space seabeds by comparison to beam patterns obtained using the numerical integration approach outlined in Appendix A. The two approaches were found to agree to better than 0.5 dB.

The plane wave reflection coefficient method (Equation (3)), and the method based on SCOOTER were implemented for a number of seabed types, the acoustic properties of which are shown in Table 1. A comparison between the magnitudes and phases of their reflection coefficients is given in Figure 1. This figure illustrates the reflection coefficients for the seabeds with frequency independent reflection coefficients (left plots) and the reflection coefficients at three different frequencies for a 1 m layer of sand over a calcarenite substrate (right plots). The four chosen seabeds offer an example of a solid with shear

Table 1: Seabed acoustic data used in propagation modelling. Acoustic characteristics are taken from Hamilton [16] and Jensen et al. [17].

Seabed	Density (kgm^{-3})	Compressional wave speed (ms^{-1})	Compressional wave attenuation (dB per wavelength)	Shear wave speed (ms^{-1})	Shear wave attenuation (dB per wavelength)
Basalt	2700	5250	0.1	2500	0.2
Calcerenite	2400	2800	0.1	1400	0.2
Sand	2034	1836	0.7	n/a	n/a
Silt	1740	1575	1	n/a	n/a

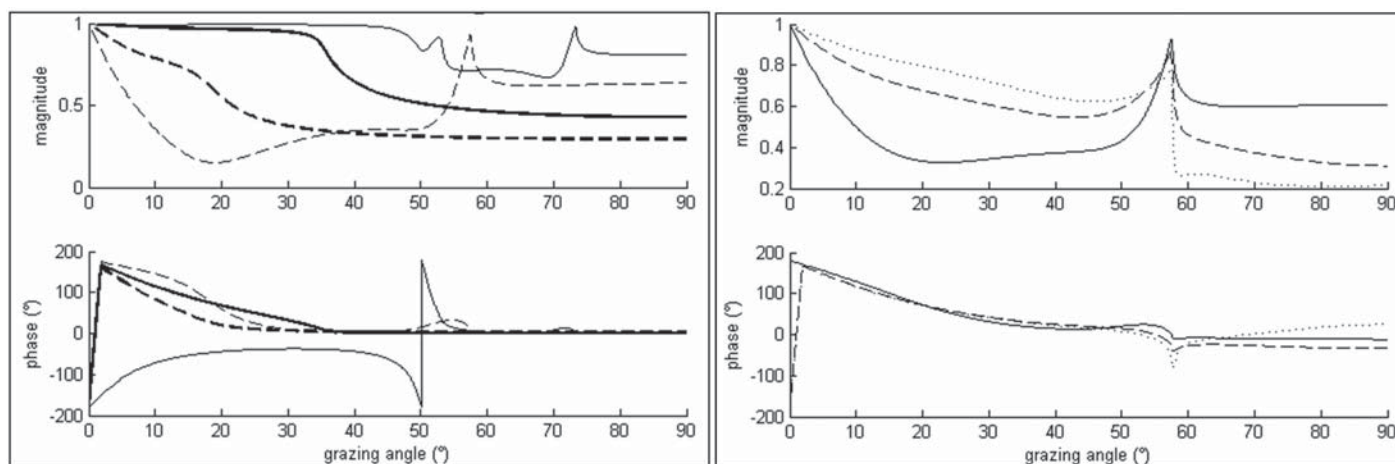


Figure 1: Reflection coefficient (top) and phase (bottom) with grazing angle for basalt, calcarenite, sand and silt half space seabeds (continuous thin, dashed thin, continuous thick and dashed thick lines, respectively in the left plot). Reflection coefficient and phase for a seabed comprising 1 m of sand over calcarenite at 100, 350 and 500 Hz (continuous, dashed and dotted lines, respectively, in the right hand plot). All values determined using the plane wave reflection coefficient calculation program, BOUNCE.

speed faster than the water column sound speed (basalt), a solid with shear speed slower than that of the water column sound speed (calcarenite) and two seabeds for which the shear effects are small and considered negligible for the purposes of this paper (sand and silt).

The analysis in Appendix B shows that for a hydrophone on the seabed, a frequency independent reflection coefficient leads to an effective beam pattern that is a function of range normalised by wavelength, rather than depending independently on these two parameters. The basalt, calcarenite, sand and silt half space seabeds have this property.

RESULTS

The results calculated using these models broadly illustrate the differences in receive beam pattern of bottom located hydrophones due to the acoustic properties of varying seabeds. In most cases the magnitude of the beam pattern varies between -5 and +5 dB. However, under certain conditions of grazing

angle, range and seabed characteristics, the received level can be up to 10 dB greater than that expected if there was no seabed reflection.

Figure 2 illustrates the variation in receive beam pattern for a hydrophone sitting on the four different seabeds, each modelled as a homogeneous half space. The far-field result was calculated using the plane wave reflection coefficient and Equation (3), whereas the other results were calculated using the numerical modelling method based on SCOOTER described above. The response for each half space was frequency independent, but range dependent, with more variation with range shown by the basalt and calcarenite seabeds than the sand and silt seabeds, which do not support shear waves (Figure 2, thick lines compared with thin lines). There was significant change in both the magnitude and angle of sidelobes in the basalt beam pattern with increased range (Figure 2, thin continuous lines). By comparison, the silt and sand receive patterns varied very little with range.

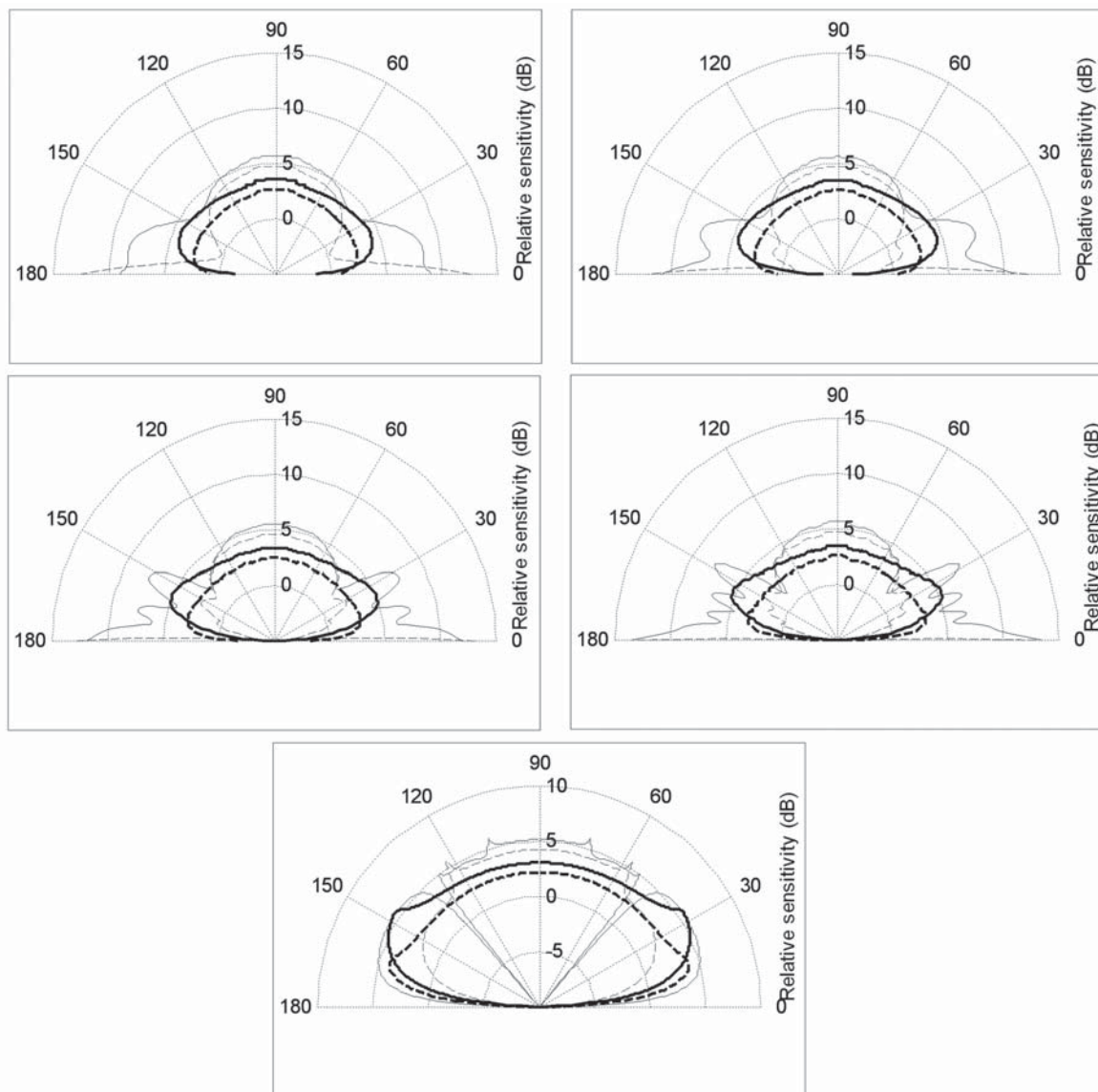


Figure 2: Hydrophone receive beam pattern for basalt (thin continuous line), calcarenite (thin dashed line), sand (thick continuous line) and silt (thick dashed line), for 3, 4, 8 and 12 wavelengths range (top left, top right, middle left and middle right, respectively) and the far field (bottom) as determined by the method using SCOOTER.

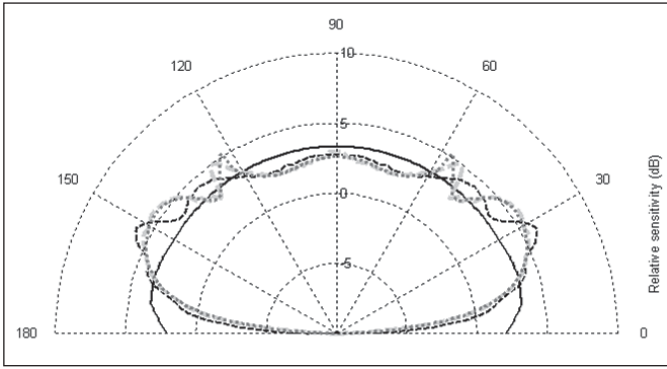


Figure 3: Hydrophone receive beam pattern for 1 wavelength of sand over calcarenite at ranges of 1 wavelength (thick continuous line), 10 wavelengths (thick dashed line), 100 wavelengths (thick grey dashed line) and the far field (thick black dotted line) as determined by method using SCOOTER.

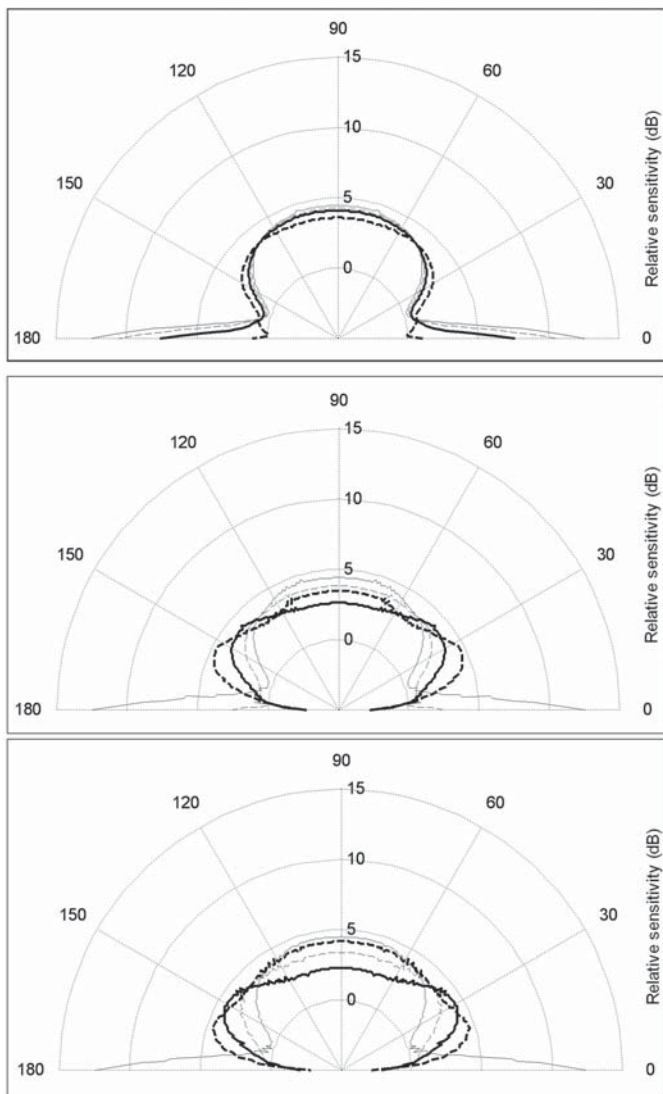


Figure 4: Hydrophone receive beam pattern for bare calcarenite (thick continuous line), then a layer of 0.5 m (thin dashed), 1 m (thick grey continuous line) and 2 m (thick grey dashed line) of sand above calcarenite for 100, 350 and 500 Hz (top, middle and bottom, respectively) at 3 wavelengths range, as determined by the method using SCOOTER.

Figure 3 illustrates the beam pattern for a hydrophone on a 1 wavelength thick layer of sand over a calcarenite substrate at 500 Hz, for different ranges (also normalised by wavelength). This shows how the pattern changes from the response at 1 wavelength range (Figure 3, thick continuous line) until by 100 wavelengths range (thin dashed line) it is very similar to the far-field, plane wave response (thin continuous line).

As the thickness of a layer of sand above a calcarenite half space is increased the beam pattern varies significantly (Figure 4, compare the different lines on each plot). At high grazing angles, near the normal to the seabed, the hydrophone response decreases with increasing thickness of sand layer, however, at lower grazing angles the response increases (Figure 4). The increased sand thickness has greater effect on the changes in beam pattern at the higher frequencies (Figure 4, compare the top plot for 100 Hz, with the bottom plot for 500 Hz).

The variation of response with range and angle from the hydrophone can be seen in Figure 5. This comparison between the responses for basalt (top image) and sand (bottom image) highlights not only the differences in complexity of beam patterns which can occur, but also the considerable variation in magnitude of response. At small grazing angles and ranges of 15-20 wavelengths a basalt seabed may display a relative response of 15 dB, while at the same angle the hydrophone located on sand would exhibit a response nearly 25 dB lower at -10 dB.

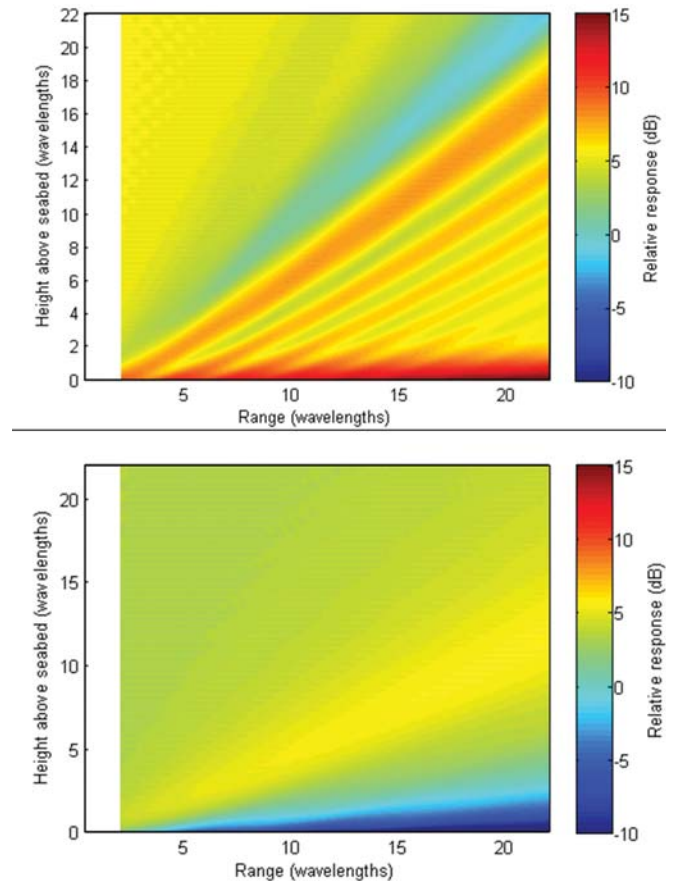


Figure 5: Relative hydrophone response as a function of source location at 500 Hz for basalt (top) and sand (bottom), as determined by the method using SCOOTER.

DISCUSSION

This study has shown that the receive beam pattern of a bottom located hydrophone can vary significantly with range, angle and frequency, with some seabeds displaying a maximum variation of over 10 dB. The variation in response for a given angle, range and frequency for two different seabed types can be as high as 25 dB. The implications for ground truthing modelled received levels and estimating the source level of underwater sounds are significant. For example, one method of localising marine animals is to use the relative received energy from multiple hydrophones [11]. If the estimated received levels do not account for variation in the received beam pattern, the uncertainty in the location of the animal can increase dramatically.

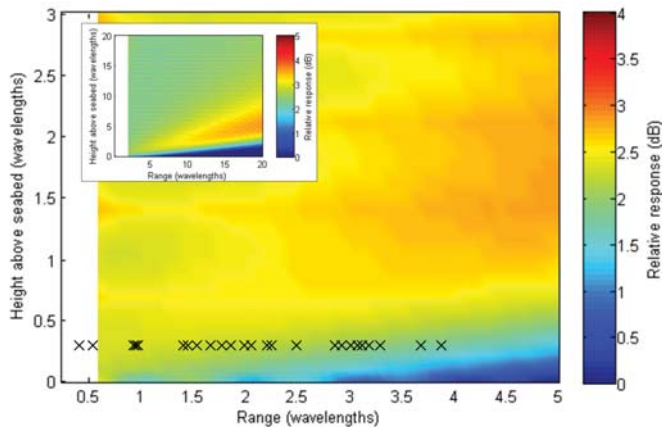


Figure 6: Relative intensity of receive beam pattern of a hydrophone located on silt seabed with range (inset, top left) with a magnification ranging between 0 and 5 wavelengths range. Black crosses mark the range of a call by a mulloway (*Argyrosomus japonicus*), as reported by Parsons et al. [19, 21].

A simple application of the effects of variations in the receive pattern can be seen in Figure 6. Mulloway (*Argyrosomus japonicus*) are a vocal species of fish and frequently found producing sounds in the Swan River, Western Australia while spawning [5, 18]. Parsons et al. [19] ranged calls of mulloway from a single hydrophone. Over 24 calls the fish was positioned at various ranges, between 1.6 and 18 m from the hydrophone. As calls of an individual fish are often considered to be comparatively constant [5, 20], the sound pressure levels of each ranged call could be considered to be a relative estimate of range. However, as the fish moved towards and away from the hydrophone it passed through different areas of the receive beam pattern. The inset in Figure 6 shows the response with range for a hydrophone located on a silt seabed similar to that of Mosman Bay, in the Swan River Western Australia, where the recordings of *A. japonicus* took place. The larger image magnifies a small section of this beam pattern for up to 5 and 3 wavelengths range on the x and y axes respectively. Parsons et al. [21] ranged the fish between approximately 0.3 and 4 wavelengths range in the x-direction and it was estimated to maintain an altitude of approximately 0.3 wavelengths or less above the riverbed, during the recording (shown by the Xs in Figure 6). These positions occurred across regions of the receive pattern which varied in response between 1.5 and 2.5 dB.

In the described case the receive pattern would have a comparatively minor effect on the received levels, producing an over estimate in source level of only 1-2 dB. However, with more reflective seabeds which support shear waves it is easy to see how a lack of understanding of the effective hydrophone receive pattern could lead to significant under-, or overestimates of the source level. This variation is an important factor, especially when assessing the environmental impacts of anthropogenic noise.

ACKNOWLEDGEMENTS

The authors would like to acknowledge the Fisheries Research and Development Corporation (FRDC) for funding of this work.

REFERENCES

- [1] H. Slabbekoorn, N. Bouton, I.V. Opzeeland, A. Coers, C.T. Cate and A.N. Poppers, "A noisy spring: the impact of globally rising underwater sound levels on fish", *Tre. Eco. Evo.* **22**(7), 419-27 (2010)
- [2] B.L. Southall, A.E. Bowles, W.T. Ellison, J.J. Finneran, R.L. Gentry, C.R. Greene Jr., D. Kastak, D.R. Ketten, J.H. Miller, P.E. Nachtigall, W. J. Richardson, J.A. Thomas and P.L. Tyack, "Marine mammal noise exposure criteria: Initial scientific recommendations", *Aqua. Mam.*, **33**(4), 411-521 (2007)
- [3] R.D. McCauley, S.R. Rennie, J.R. Hughes, and A.J. Duncan, "Transmission of marine seismic signals in Australian waters". *Bioacoust.* **17**, 130-132 (2008)
- [4] D.H. Cato, R.D. McCauley and M. Noad, Passive acoustics as a key to the study of marine animals, in *Sounds in the Seas: Introduction to Acoustical Oceanography*, (editor H. Medwin), Chapter 13, Cambridge University Press, 2005
- [5] M.J.G. Parsons, *An investigation into active and passive acoustic techniques to study aggregating fish species*, PhD Thesis, Curtin University of Technology, Western Australia, 2010
- [6] R.D. McCauley, C.P. Salgado Kent, C.J.K. Burton and C. Jenner, "Blue whale calling in Australian waters", *J. Acoust. Soc. Am.*, **120**(5), pp. 3266 (2006)
- [7] A. Širović, J. A. Hildebrand and S. M. Wiggins, "Blue and fin whale call source levels and propagation range in the Southern Ocean," *J. Acoust. Soc. Am.*, **122**, 1208-1215 (2007)
- [8] R.J. Urlick, *Principles of underwater sound*, MacGraw-Hill, New York, 1983
- [9] A.J. Duncan and R.D. McCauley, "Environmental impact assessment of underwater sound: Progress and pitfalls", *Proceedings of Acoustics 2008*, Geelong, Victoria, Australia, 24-26 November 2008
- [10] P.C. Etter, *Underwater acoustic modelling and simulation*, 3rd edition, Spon Press, London, 2003
- [11] D.H. Cato, "Simple methods of estimating source levels and locations of marine animal sounds" *J. Acoust. Soc. Am.* **104**, 1667-78 (1998)
- [12] M.B. Porter, *Acoustics Toolbox*, available from <http://oalib.hlsresearch.com/Modes/AcousticsToolbox/>
- [13] A.J. Duncan and A.L. Maggi, "A consistent, user friendly interface for running a variety of underwater acoustic propagation codes", *Proceedings of the First Australasian Acoustical Societies' Conference*, Christchurch, New Zealand, 20-22 November 2006, pp 471-477
- [14] L.M. Brekovskikh and Y.P. Lysanov, *Fundamentals of ocean acoustics*, Springer, New York, 2002

- [15] L.E. Kinsler, *Fundamentals of acoustics*, 4th edition, Wiley, New York, 2000
- [16] E.L. Hamilton, "Geoacoustic modelling of the sea floor", *J. Acoust. Soc. America*, **68**,(5), 1313-1340 (1980)
- [17] F.B. Jensen, W.A. Kuperman, M.B. Porter and H. Schmidt, *Computational ocean acoustics*, Springer-Verlag, New York, 2000
- [18] M.J.G. Parsons, R.D. McCauley and M.C. Mackie, "Spawning sounds of the mulloway (*Argyrosomus japonicus*)", *Proceedings of the First Australasian Acoustical Societies' Conference*, Christchurch, New Zealand. 20-22 November 2006, pp. 401-6.
- [19] M.J.G. Parsons, R.D. McCauley, M.C. Mackie and A.J. Duncan, "A comparison of techniques for ranging close-proximity mulloway (*Argyrosomus japonicus*) calls with a single hydrophone" *Acoust. Australia*. **38**(3), 145-151 (2010)
- [20] M.A. Connaughton, M.H. Taylor, and M.L. Fine, "Effects of fish size and temperature on weakfish disturbance calls: Implications for the mechanism of sound generation", *Journ. Exp. Bio.* **203**, 1503-1512 (2000)
- [21] M.J.G. Parsons, R.D. McCauley, M.C. Mackie, P.J. Siwabessy and A.J. Duncan, "Localisation of an individual mulloway (*Argyrosomus japonicus*) within a spawning aggregation and their behavioural characteristics throughout a diel spawning period" *ICES J. Mar. Sci.* **66**, 1007-14 (2009)
- [22] W.H. Press, S.A. Teukolsky, W.T. Vetterling and B.P. Flannery, *Numerical recipes, the art of scientific computing*, 3rd edition, Cambridge University Press, New York, 2007

APPENDIX A

Numerical integration computation of the effective beam pattern of a hydrophone located on a half space seabed

To verify the results obtained using the method detailed in the body of this paper, an alternative numerical approach was developed, based on the integral transform methods described in Jensen et al. [17], chapters 2 and 4. This approach is outlined here.

The acoustic field due to a source in a horizontally stratified fluid medium can be represented by

$$\psi(r, z) = \int_{-\infty}^{\infty} S_{\omega} G_{\omega}(k_r, z, z_s) H_0^{(1)}(k_r r) k_r dk_r \quad (A1)$$

where z and z_s are respectively the vertical positions of the receiver and source, r is horizontal range, k_r is the horizontal wavenumber, S_{ω} is the wavenumber spectrum of the source, and ψ is the displacement potential. G_{ω} is the solution of the corresponding depth equation which, for a fluid medium of constant density, is

$$\left[\frac{d^2}{dz^2} + (k^2 - k_r^2) \right] G_{\omega}(k_r, z, z_s) = \frac{\delta(z - z_s)}{2\pi} \quad (A2)$$

Here k is the acoustic wavenumber and a time dependence of $\exp(-i\omega t)$ has been assumed. For an elastic medium the result involves the sum of compressional wave and shear wave potentials, each of which satisfies equations analogous to (A1) and (A2).

The case of interest here is for a uniform fluid water column of infinite depth, sound speed c_1 and density ρ_1 over an infinite elastic seabed with compressional wave speed c_{p2} , shear

speed c_{s2} and density ρ_2 . The z coordinate is taken as positive downwards, with $z = 0$ at the seabed. For this case the Greens function in the water column, $G_{\omega 1}$, is given by:

$$G_{\omega 1}(k_r, z, z_s) = A_1 \exp(-ik_{z1}z) - \frac{\exp(-ik_{z1}|z - z_s|)}{4\pi k_{z1}} \quad (A3)$$

where $k_{z1} = \sqrt{k_1^2 - k_r^2}$ and $k_1 = \omega/c_1$ is the acoustic wavenumber. The second term in Equation (A3) represents the signal coming directly from the source whereas the first term is the signal reflected from the seabed.

The compressional wave and shear wave Greens functions in the seabed are given respectively by:

$$G_{\omega p2}(k_r, z, z_s) = A_2 \exp(ik_{z2}z) \quad (A4)$$

$$G_{\omega s2}(k_r, z, z_s) = B_2 \exp(ik_{z2}z) \quad (A5)$$

with $k_{z2} = \sqrt{k_2^2 - k_r^2}$, $\kappa_{z2} = \sqrt{\kappa_2^2 - k_r^2}$, $k_2 = \omega/c_{p2}$ and $\kappa_2 = \omega/c_{s2}$.

The constants A_1 , A_2 and B_2 are determined from the boundary conditions at the seabed interface which require continuity of vertical stress and vertical displacement, and vanishing horizontal stress.

An expression for the displacement potential can then be obtained by solving for A_1 , substituting the result back into Equation (A3), $S_{\omega} = \frac{-4\pi}{\rho\omega^2}$, which corresponds to a point source with unit pressure amplitude at 1 m, and evaluating Equation (A1). Making use of the relationship between pressure and displacement potential, $p = \rho\omega^2\psi$, then leads to the following expression for the received pressure at the seabed ($z = 0$):

$$p(r, 0) = \frac{i}{2} \int_{-\infty}^{\infty} (1 + \Re(k_r)) \frac{\exp(ik_{z1}z_s)}{k_{z1}} H_0^{(1)}(k_r r) k_r dk_r \quad (A6)$$

Here $\Re(k_r)$ is the plane wave reflection coefficient, which is given by

$$\Re(k_r) = \frac{T_1 - T_2}{T_1 + T_2} \quad (A7)$$

where $T_1 = \rho_2 k_{z1} \{ (2k_r^2 - k_2^2)^2 + 4k_r^2 k_{z2} \kappa_{z2} \}$, $T_2 = \rho_1 k_{z2} \kappa_{z2}^4$.

The effective beam pattern is obtained by referring the received pressure back to a distance of 1m from the source assuming spherical spreading, giving

$$b(r, z_s) = R |p(r, 0)| \\ = R \left| \frac{i}{2} \int_{-\infty}^{\infty} (1 + \Re(k_r)) \frac{\exp(ik_{z1}z_s)}{k_{z1}} H_0^{(1)}(k_r r) k_r dk_r \right| \quad (A8)$$

where $R = \sqrt{r^2 + z_s^2}$ is the slant range between source and receiver. Note that the integration range in Equation (A8) includes the evanescent region where $|k_r| > |k_1|$ and k_{z1} is imaginary. It is important that this region is included when numerically evaluating Equation (A8) because Scholte interface waves, which decay exponentially either side of the

interface, occur in the evanescent region and are an important contributor to the received field when the source and receiver are both close to the seabed.

Brekhovskikh and Lysanov [14] (p. 88) give an exact integral formula for the reflected wave from a point source over a fluid seabed. For the limiting case of a receiver on the seabed, their result is identical to Equation (A6), but with $1+\mathfrak{R}(k_r)$ replaced by $\mathfrak{R}(k_r)$ (because only the reflected wave is considered, whereas Equation (A6) gives the total field) and Equation (A7) replaced by an appropriate expression for the plane wave reflection coefficient of a fluid-fluid interface. They go on to derive analytic formulae for the received signal in terms of geometrically reflected and lateral waves, however their derivation requires assumptions that are invalid for a receiver located on the seabed, so for the case of interest here it is necessary to proceed by numerical integration of Equation (A8). This was achieved using the extended midpoint rule (Press et. al. [22]), with the integration step being progressively reduced until convergence was obtained.

APPENDIX B

Invariance of the effective beampattern for constant range/wavelength ratios

The frequency dependence of Equation (A8) can be made explicit by changing the integration variable to $u = k_r / \omega$, and making use of the relation $k_1 = \omega / c_1$, leading to:

$$b(r, z_s) = R|p(r, 0)| \\ = \omega R \left| \frac{i}{2} \int_{-\infty}^{\infty} (1 + \mathfrak{R}(\omega u)) \frac{\exp(i v \omega z_s)}{v} H_0^{(1)}(\omega r) u du \right| \quad (B1)$$

$$\text{where } v = \sqrt{\frac{1}{c_1^2} - u^2}.$$

With these definitions u and v are independent of range and frequency. Using Equation (A7) it is straightforward to show that $\mathfrak{R}(\omega u)$ is independent of ω for an elastic half space seabed. This is true for a seabed without attenuation, but also for a seabed with attenuation that is proportional to frequency. The effects of attenuation can be included in the usual way by making the compressional and shear wave speeds, and hence k_2 and κ_2 complex (Jensen et. al. [17], pp 33-34).

If ωR is held constant, then for the same beam angle, ωr and ωz_s will also be constant, and the effective beam pattern computed by (B1) is invariant. The acoustic wavelength in the water column is given by $\lambda = 2\pi c_1 / \omega$, so the effective beam pattern will be unchanged with changes in frequency if r / λ is held constant.

Note that this invariance requires the hydrophone to be on the seabed, and the seabed reflection coefficient to be independent of frequency. It is not generally the case for a hydrophone located above the seabed or for a more complicated seabed with a frequency dependent reflection coefficient.

BACKGROUND NOISE AFFECTS THE TASTE OF FOODS

The level of background noise affects both the intensity of flavour and the perceived crunchiness of foods, researchers have found. Blindfolded diners assessed the sweetness, saltiness, and crunchiness, as well as the overall flavour, of foods as they were played white noise. Louder noise reduced the reported sweetness or saltiness, and increased the impression of crunchiness. The research is reported in the industry journal Food Quality and Preference.

It may go some way to explaining why airline food is notoriously bland, a phenomenon that drives airline catering companies to season their foods heavily. Researchers from the Unilever Research and Development laboratories in the Netherlands and the University of Manchester, UK, say that there is a general opinion that airline foods are less than fantastic. Airlines do their best, but the researchers wondered if there were other reasons why the food would not be so good. One thought was that perhaps the background noise had some impact. NASA gave their space explorers very strong-tasting foods, because for some reason they could not food very strongly. Again, perhaps the background noise was affecting their perception. There was no previous research on this, so the team started to investigate whether the hunch was correct.

In a comparatively small study, 48 participants were fed sweet foods such as biscuits, or salty ones such as crisps, while listening to silence or noise through headphones. They then rated the intensity of the flavours, and rated their liking of the foods presented. In noisier settings, foods were rated less salty or sweet than they were in the absence of background noise, but were rated to be more crunchy. The evidence points to the effect being down

to where the person's attention was focused. If the background noise was loud it might draw your attention, and thus away from the food.

Also in the group's findings there is the suggestion that the overall satisfaction with the food was correlated with the degree to which diners liked what they were hearing, and this is a finding the researchers are pursuing in further experiments.

In the words of the experimenters (from the School of Psychological Sciences, University of Manchester, UK, and Unilever Research and Development, Vlaardingen, Netherlands), they investigated the effects of auditory background noise on the perception of gustatory food properties (sugar level, salt level), food crunchiness and food liking. Participants blindly consumed different foods whilst passively listening to either no sound, or quiet or loud background white noise. The foods were then rated in terms of sweetness, saltiness and liking (experiment 1) or in terms of overall flavour, crunchiness and liking (experiment 2). Reported sweetness and saltiness was significantly lower in the loud compared with the quiet sound conditions, but crunchiness was reported to be more intense. This suggests that food properties unrelated to sound (sweetness, saltiness) and those conveyed via auditory channels (crunchiness) are differentially affected by background noise. A relationship between ratings of the liking of background noise and ratings of the liking of the food was also found in experiment 2. It was concluded that background sound unrelated to food diminishes gustatory food properties (saltiness, sweetness) which is suggestive of a cross-modal contrasting or attentional effect, whilst enhancing food crunchiness.